10.1098/rspa.2000.0637

THE ROYAL SOCIETY

On effective resistivity and related parameters for periodic checkerboard composites

By R. V. Craster

Department of Mathematics, Imperial College of Science, Technology and Medicine, London SW7 2BZ, UK

Received 20 March 2000; accepted 20 June 2000

An approach for finding the effective properties of two-dimensional periodic rectangular checkerboard media is presented; it is demonstrated that one can take a relatively simple model problem, an appropriate system of joined quarter planes, and that after appropriate conformal transformation one can use this to solve for either periodic or doubly periodic structures. Illustrative calculations involving three-phase media are presented that, in limiting cases, recover earlier analyses. Useful asymptotic relations are also given.

Keywords: effective parameters; complex analysis; composite materials

1. Introduction

We consider here a class of two-dimensional rectangular periodic composites; each rectangular cell can be composed of up to four different phases. The aim is to find the effective parameters associated with such a structure for linear materials in, say, electrostatics; in later sections, for algebraic simplicity and clarity, we shall deal with three different phases.

The evaluation of effective parameters for related structures composed of two differing phases has a long history with many different approaches, it is only possible to give here a flavour of each of them, these are useful asymptotic results; representations and theorems for special cases (Bruggeman 1935; Keller 1963, 1964, 1987; Dykhne 1971; Mendelson 1975; Milton & Golden 1990), or network resistance analogies (Borcea & Papanicolaou 1998); numerical work using integral equations (Gautesen 1988), or complex power series (Milton *et al.* 1981) or other expansion methods (Helsing 1991); and effective medium approximations or other methods (Clark & Milton 1995) for establishing upper and lower bounds for the effective properties (Torquato 1991). Some of these methods also allow one to progress to considering nonlinear composites (Talbot & Willis 1994).

Exact solutions for this class of problems, even for two-phase media, are quite rare. There are, of course, the classical analyses of Rayleigh (1892) and Maxwell (1904), and more recent work for square (Berdichevski 1985) or rectangular (Obnosov 1996, 1999*a*) checkerboard structures, and biperiodic cylindrical inclusions (Mityushev 1997). The latter authors use complex analysis to formulate generalized Riemann boundary-value problems known as $\mathcal{R}$-linear conjugation, or Markushevich problems. In general, the analysis of these $\mathcal{R}$-linear conjugation problems appears to

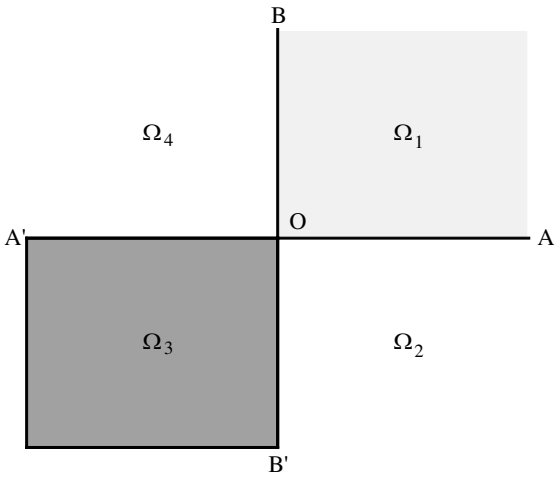

Figure 1. The four-lobe fan in the physical plane.

have placed an effective block upon further progress; considerable ingenuity having been required to solve for even these simple geometries. Here we develop an inverse method that completely bypasses that approach, and leads relatively easily to more general results (for more phases) that encompass these earlier checkerboard results. In essence we take a solution for a simple geometry, a four-lobe fan, and then use conformal mappings to this structure to deduce the general form for the equivalent periodic and biperiodic media. Thus we are now only limited by the algebra associated with the four-lobe fan; the method itself can also be extended to other regular biperiodic structures, such as rhomboid tilings. An advantage of obtaining exact solutions, albeit to relatively simple geometrical structures, is that these then provide sound checking mechanisms for numerical schemes and may also highlight asymptotic schemes of value in more complex geometrical or higher-dimensional structures.

We consider here four-phase piecewise continuous stationary media that can be represented in terms of a vector field that is both solenoidal and irrotational; this encompasses several physical scenarios in electro- or magnetostatics, heat flow, hydrology and elasticity. The language of the electrostatic analogy is used in later sections. In each phase distinguished by the subscript p, where $p = 1, \ldots, 4$, we define a vector field $\boldsymbol{w}_p = (w_{px}, w_{py})$ of the horizontal and vertical components w_x, w_y such that

$$\nabla \cdot \boldsymbol{w}_p = 0 \quad \text{and} \quad \nabla \times \boldsymbol{w}_p = 0.$$

It is most convenient to use complex variables, that is $z = x + \mathrm{i}y$ and $w_p(z) = w_{px} - \mathrm{i}w_{py}$. In each sector, Ω_p $(p = 1, \ldots, 4)$, the piecewise analytic functions $w_p(z)$ are defined. Since we have eigenproblems the results depend crucially upon the singularity behaviour at each vertex, from physical considerations these functions have, at most, integrable singularities there. The boundary conditions between each phase are that the normal components of $\boldsymbol{w}_p$ are continuous across each boundary, and that the tangential components of $\rho_p \boldsymbol{w}_p$ are similarly continuous; the constant parameters ρ_p correspond to a phase property of each medium. For ease of analysis these parameters are taken to be real in the remainder of these notes, although this is not a restriction upon the method.

The plan of this paper is that in § 2 we give the general solution to a simple four-lobe fan structure. In §§ 3 and 4 we give the mappings, and analysis, required for displaced flake and checkerboard structures. In § 5 we make comparisons with two-phase structures and square checkerboards and give asymptotic results for 'long thin' biperiodic structures. We conclude in § 6.

2. The four-lobe fan

As we shall ultimately conformally map into the four-lobe fan, the geometry of which is shown in figure 1, from periodic and doubly periodic structures, we shall pose the problem in an intermediate ζ-plane; later, $\zeta(z)$ will define an appropriate map. For algebraic ease we shall consider $\rho_2 \equiv \rho_4$ and, thus, that the materials in Ω_2 and Ω_4 are identical; this retains some symmetry in the problems.

In terms of the complex representation adopted here, and the lettering of figure 1, the boundary conditions are that

$$\mathrm{Im}[\mathrm{i}(\rho_1 w_1 - \rho_2 w_2)] = 0, \qquad \mathrm{Im}[w_1 - w_2] = 0, \qquad \text{on OA}, \tag{2.1}$$

$$\mathrm{Im}[\mathrm{i}(\rho_4 w_4 - \rho_3 w_3)] = 0, \qquad \mathrm{Im}[w_4 - w_3] = 0, \qquad \text{on OA}', \tag{2.2}$$

$$\mathrm{Im}[\mathrm{i}(w_4 - w_1)] = 0, \qquad \mathrm{Im}[\rho_4 w_4 - \rho_1 w_1] = 0, \qquad \text{on OB}, \tag{2.3}$$

$$\mathrm{Im}[\mathrm{i}(w_2 - w_3)] = 0, \qquad \mathrm{Im}[\rho_2 w_2 - \rho_3 w_3] = 0, \qquad \text{on OB}'. \tag{2.4}$$

These conditions are probably most easily reduced to algebraic conditions and then solved, using ideas related to Mellin transforms defined in the complex ζ-plane as in, say, Craster (1997).

We search for eigensolutions of the form $\tilde{w}_k = A_k(\lambda)\zeta^{2\lambda}$ $(k = 1, \ldots, 4)$, for some parameter λ to be determined; the $\tilde{\cdot}$ distinguishes a single eigensolution from the full solution w_k that is formed from two eigensolutions. Equations (2.1)–(2.4) describe an eigenproblem with an infinite number of possible solutions. To fix upon a specific solution we also require conditions set at the origin or at infinity. For physical reasons associated with our later periodic and doubly periodic examples, we restrict λ such that $|2\lambda| < 1$, and aim to find those two solutions for which $\tilde{w}_k$ is bounded at the origin, or at infinity, respectively. The aim is to identify λ as an eigenvalue and also the general form that the constants $A_k(\lambda)$ must take. To streamline notation we introduce Δ, γ, ϵ_2 and ϵ_3 as

$$\Delta = \frac{(\epsilon_3 - \epsilon_2)}{(1+\epsilon_2)(1+\epsilon_3)}, \qquad \tan \pi\gamma = \sqrt{\frac{1+\Delta}{1-\Delta}}, \qquad \epsilon_2 = \frac{\rho_2}{\rho_1}, \qquad \epsilon_3 = \frac{\rho_3}{\rho_2}.$$

Substituting the representation for $\tilde{w}_k$ into the boundary conditions, eight algebraic equations for the A_k, and their conjugates, are deduced, and these are solved straightforwardly. In the process of which an equation for λ is found as

$$4\Delta^2(1 + \cos 2\lambda\pi) = (1 - \cos 4\lambda\pi), \tag{2.5}$$

from which

$$\lambda = (1/\pi)\sin^{-1}\Delta.$$

The other eigensolution is similarly found with eigenvalue $-[1/\pi]\sin^{-1}\Delta$; these together satisfy the required behaviour.

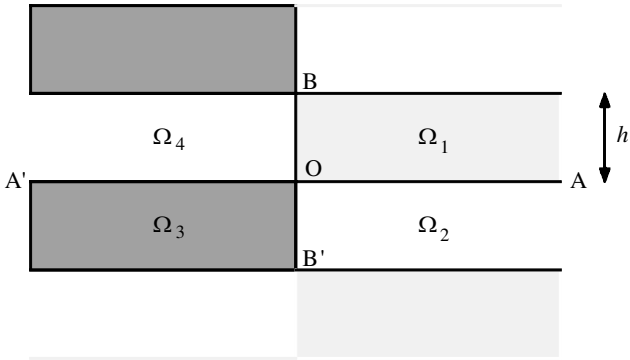

Figure 2. The geometry for the periodic problem in the physical plane.

An alternative, and arguably more elegant, method is to rewrite the boundary-value problem (2.1)–(2.4) as a Riemann–Hilbert problem (Craster & Obnosov 2000). Ultimately this avoids the explicit treatment of simultaneous equations for the $A_k(\lambda)$. Recently, Craster & Obnosov (2000) have used this approach (Appendix A of that article), which allows us to proceed there with consideration of four arbitrary piecewise constant phases.

The solutions for the two relevant eigensolutions are used to construct the functions w_k. These w_k are found as

$$w_1(\zeta) = \alpha \mathrm{e}^{\mathrm{i}\pi\gamma}\zeta^{-2\lambda} + \beta \mathrm{e}^{-\mathrm{i}\pi\gamma}\zeta^{+2\lambda}, \tag{2.6}$$

$$w_2(\zeta) = ([1+\epsilon_2] - \mathrm{i}[1-\epsilon_2]\mathrm{e}^{-\mathrm{i}\pi\lambda})\frac{\alpha \mathrm{e}^{\mathrm{i}\pi\gamma}}{2\epsilon_2}\zeta^{-2\lambda} + ([1+\epsilon_2] + \mathrm{i}[1-\epsilon_2]\mathrm{e}^{\mathrm{i}\pi\lambda})\frac{\beta \mathrm{e}^{-\mathrm{i}\pi\gamma}}{2\epsilon_2}\zeta^{+2\lambda}, \tag{2.7}$$

$$\begin{aligned} w_3(\zeta) = \frac{1}{4\epsilon_3\epsilon_2}[&(1+\epsilon_3)([1+\epsilon_2] - \mathrm{i}[1-\epsilon_2]\mathrm{e}^{-\mathrm{i}\pi\lambda}) + (\epsilon_3 - 1)\mathrm{e}^{-2\mathrm{i}\pi\lambda} \\ &\times ([1+\epsilon_2] + \mathrm{i}[1-\epsilon_2]\mathrm{e}^{\mathrm{i}\pi\lambda})]\alpha \mathrm{e}^{\mathrm{i}\pi\gamma}\zeta^{-2\lambda} + [(1+\epsilon_3)([1+\epsilon_2] + \mathrm{i}[1-\epsilon_2]\mathrm{e}^{\mathrm{i}\pi\lambda}) \\ &+ (\epsilon_3 - 1)\mathrm{e}^{2\mathrm{i}\pi\lambda}([1+\epsilon_2] - \mathrm{i}[1-\epsilon_2]\mathrm{e}^{-\mathrm{i}\pi\lambda})]\beta \mathrm{e}^{-\mathrm{i}\pi\gamma}\zeta^{+2\lambda}, \end{aligned} \tag{2.8}$$

$$w_4(\zeta) = ([1+\epsilon_2] + \mathrm{i}[1-\epsilon_2]\mathrm{e}^{\mathrm{i}\pi\lambda})\frac{\alpha \mathrm{e}^{\mathrm{i}\pi\gamma}}{2\epsilon_2}\zeta^{-2\lambda} + ([1+\epsilon_2] - \mathrm{i}[1-\epsilon_2]\mathrm{e}^{-\mathrm{i}\pi\lambda})\frac{\beta \mathrm{e}^{-\mathrm{i}\pi\gamma}}{2\epsilon_2}\zeta^{+2\lambda}. \tag{2.9}$$

These solutions can be verified readily by substitution back into the boundary conditions. The two real parameters α and β that appear are unknown, and in each following example these are found by applying additional flux conditions in each cell. The branch cuts for $\zeta^{\pm 2\lambda}$ lie along OA′ (0 to $-\infty$) and $|\arg(\zeta)| < \pi$. These solutions are instrumental in the following sections.

3. Periodic solutions

Now let us consider the strip-like geometry in the z-plane shown in figure 2, that is, we have semi-infinite strips of height h that periodically repeat. Under the action of the mapping $\zeta(z) = \tanh(\pi z/2h)$ this harmonic problem maps the points to those shown in figure 3; the points A and A′, which were at $\pm\infty$ in the physical plane, now map to ± 1. We now consider how this affects the continuity boundary conditions,

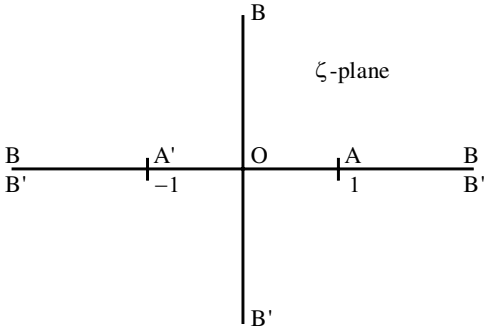

Figure 3. The positions of the points in the ζ-plane.

clearly along OA, OA′, OB and OB′ we require the continuity conditions to hold. If the problem is periodic, then the continuity conditions hold along AB, AB′ and also along A′B, A′B′, thus in the ζ-plane we recover precisely the four-lobe fan solution, but with $\zeta(z)$ now redefined to be the tanh function. Thus we have immediately that $w_1(\zeta), \ldots, w_4(\zeta)$ are just equations (2.6)–(2.9) again. Note the solutions are bounded at infinity and have, at most, integrable singularities at the origin, as we also require.

The real constants α, β that appear in these formulae must now be determined using flux conditions across each periodic cell:

$$a = \frac{1}{2h}\int_{-h}^{h} \mathrm{Re}[w_p(0,y)]\,\mathrm{d}y, \quad b = \frac{1}{2l}\int_{-l}^{l} \mathrm{Im}[w_p(x,0)]\,\mathrm{d}x, \quad \text{as } l \to \infty. \tag{3.1}$$

It is convenient to evaluate each vertical and horizontal integral along the axes, and there is no loss of generality in doing so. The subscript p takes the appropriate value depending on which phase we are in, and w_p has the arguments (x, y) associated with z. Performing these integrals we obtain

$$\alpha = \frac{\epsilon_2}{(1+\epsilon_2)\cos\pi\gamma}\left(a + \frac{b}{\cos\pi\lambda}\right), \qquad \beta = \frac{\epsilon_2}{(1+\epsilon_2)\cos\pi\gamma}\left(a - \frac{b}{\cos\pi\lambda}\right). \tag{3.2}$$

We are now in a position to be able to calculate some effective parameters; the effective resistivities (these are the reciprocal of the conductivities) along the x- and y-axes are

$$\rho_y = \frac{1}{2hb}\int_{-h}^{h} \mathrm{Im}[\rho_p w_p(0,y)]\,\mathrm{d}y \quad \text{and} \quad \rho_x = \frac{1}{2la}\int_{-l}^{l} \mathrm{Re}[\rho_p w_p(x,0)]\,\mathrm{d}x \tag{3.3}$$

in the limit as $l \to \infty$. Evaluating these integrals (see Appendix A) one finds that

$$\rho_x = \rho_2(1+\Delta), \qquad \rho_y = \frac{\rho_2}{1-\Delta}. \tag{3.4}$$

Other effective parameters, such as an effective resistivity tensor, can be deduced. In the complex notation we evaluate

$$\rho = \int_\Omega \rho_p w_p(z)\,\mathrm{d}A \Big/ \int_\Omega w_p(z)\,\mathrm{d}A = \frac{a\rho_x - \mathrm{i}b\rho_y}{a - \mathrm{i}b}, \tag{3.5}$$

with $\Omega = \sum_p \Omega_p$, and ρ_p, w_p take their respective values in each Ω_p. That is, we, in some sense, average over the area of the periodic cell. The representation of ρ

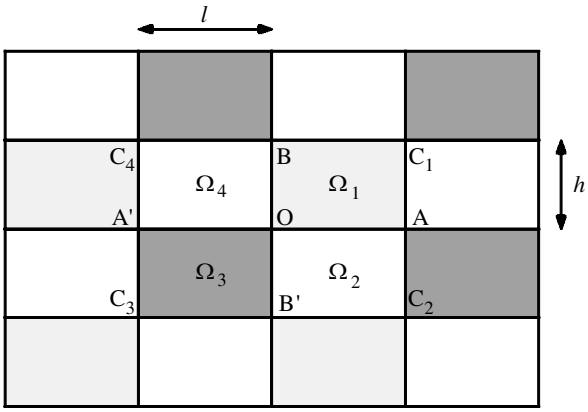

Figure 4. The geometry of the rectangular checkerboard in the physical plane.

in (3.5) as $[a\rho_x - \mathrm{i}b\rho_y]/[a - \mathrm{i}b]$ can be shown to be valid for the doubly periodic situation too and we elaborate on this at the end of § 4. The resulting complex ρ is $\rho = \rho_{xx} - \mathrm{i}\rho_{xy} = \rho_{yy} + \mathrm{i}\rho_{yx}$, where ρ_{ij} are the components of an effective resistivity tensor.

The effective energy dissipation is

$$D = \frac{1}{2lh}\int_{\Omega} \rho_p |w_p(z)|^2 \,\mathrm{d}A = \rho_2\left[a^2(1+\Delta) + \frac{b^2}{(1-\Delta)}\right]; \tag{3.6}$$

this is evaluated directly using integrals that appear in Obnosov (1996).

Several special cases emerge in the situations when phase properties are coincident; these parallel the cases considered in § 5 *b* and are not explicitly given here. There are also further simplifications if one phase is either perfectly conducting or has infinite resistance.

4. Doubly periodic solutions

Now let us consider the geometry in the z-plane shown in figure 4, that is, a collection of doubly periodic repeated rectangular cells of width l and height h under the action of the mapping

$$\hat{\zeta}(z) = \mathrm{sn}((K(m)z/l) \mid m).$$

The function 'sn' is the Jacobi elliptic sinus function (Lawden 1989), $K(m)$ is the complete elliptic integral of the first kind, and the parameter m is implicitly found from $K(m)/K(1-m) = l/h$. A simple and accurate approximation for $h/l < 1$ is that $m \sim 1 - 16\exp(-\pi l/h)$ (cf. figure 6), otherwise one can find m numerically using standard root-finding algorithms. Under the action of the elliptic sinus, this harmonic problem maps to that shown in figure 5. This is *not* the same as the simple four-lobe problem treated earlier but it is closely related, the only difference being the cuts along $[-1/\sqrt{m}, -1]$ and $[1, 1/\sqrt{m}]$. The limit as $m \to 1$ connects directly with the periodic examples of § 3 as then

$$\mathrm{sn}((K(m)z/l) \mid m) \to \tanh\left(\frac{\pi z}{2h}\right),$$

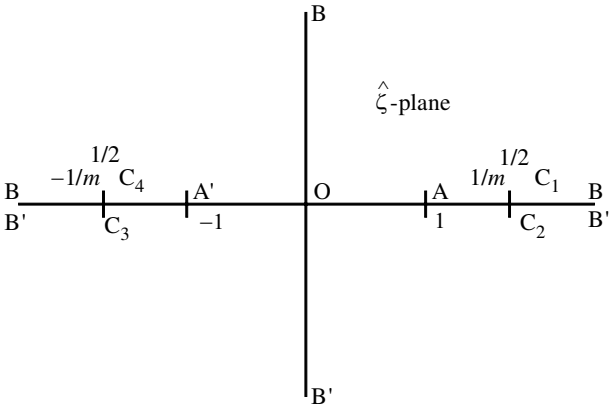

Figure 5. The positions of the points in the $\hat{\zeta}$-plane.

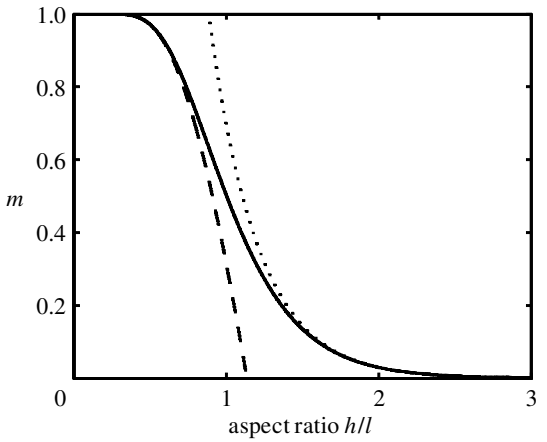

Figure 6. The exact (solid line) and asymptotic (dashed and dotted lines) expressions for m versus h/l (for $h \ll l$ and $h \gg l$).

and the cuts disappear. The doubly periodic nature of the problem is manifest in the $\hat{\zeta}$-plane, as for the continuity conditions we require

$$\mathrm{Im}[w_1]_{\mathrm{BC}_1} = \mathrm{Im}[w_2]_{\mathrm{B'C}_2}, \qquad \mathrm{Im}[\mathrm{i}\rho_1 w_1]_{\mathrm{BC}_1} = \mathrm{Im}[\mathrm{i}\rho_2 w_2]_{\mathrm{B'C}_2}, \tag{4.1}$$

$$\mathrm{Im}[w_4]_{\mathrm{BC}_4} = \mathrm{Im}[w_3]_{\mathrm{B'C}_3}, \qquad \mathrm{Im}[\mathrm{i}\rho_1 w_4]_{\mathrm{BC}_4} = \mathrm{Im}[\mathrm{i}\rho_3 w_3]_{\mathrm{B'C}_3}, \tag{4.2}$$

and these conditions are automatically satisfied by solving the four-lobe fan problem in the $\hat{\zeta}$-plane. However, we also have the conditions

$$\mathrm{Im}[w_1]_{\mathrm{AC}_1} = \mathrm{Im}[w_4]_{\mathrm{A'C}_4}, \qquad \mathrm{Im}[\rho_1 w_1]_{\mathrm{AC}_1} = \mathrm{Im}[\rho_4 w_4]_{\mathrm{A'C}_4}, \tag{4.3}$$

$$\mathrm{Im}[w_2]_{\mathrm{AC}_2} = \mathrm{Im}[w_3]_{\mathrm{A'C}_3}, \qquad \mathrm{Im}[\rho_2 w_2]_{\mathrm{AC}_2} = \mathrm{Im}[\rho_3 w_3]_{\mathrm{A'C}_3}; \tag{4.4}$$

that is, we must correctly connect the values of the functions on the upper (lower) edges of each cut. To connect this problem with the four-lobe one, when we are upon the cut we must take values on the imaginary ζ-axis, while the remaining boundaries

remain real, or imaginary. This is achieved by taking the transformation

$$\zeta(z) = \left[\frac{\hat{\zeta}^2(z)(1-m\hat{\zeta}^2(z))}{(1-\hat{\zeta}^2(z))}\right]^{1/2} = \left[\frac{1-\mathrm{cn}((2Kz/l)\mid m)}{1+\mathrm{cn}((2Kz/l)\mid m)}\right]^{1/2}, \tag{4.5}$$

where cn is the Jacobi elliptic cosine function (Lawden 1989). Now, the eigenproblem posed in terms of ζ *is* solved using the four-lobe problem; the periodic problem treated earlier does not require this last transformation. There is a minor complication in that this mapping leads to two four-lobe problems, but it is the continuity conditions that are crucial. Moreover, the solution has, at most, integrable singularities at the corner points of each cell, as we require. Thus the solutions for w_p are equations (2.6)–(2.9) again, with ζ redefined as (4.5). Applying the flux conditions (3.1) (but without requiring $l \to \infty$) we find that

$$\alpha = \frac{\epsilon_2}{(1+\epsilon_2)}\frac{\cos\pi\lambda}{\sin\pi\gamma}\frac{(a\sigma(1-m)+b\sigma(m))}{(1-\Delta)}, \tag{4.6}$$

$$\beta = \frac{\epsilon_2}{(1+\epsilon_2)}\frac{\cos\pi\lambda}{\sin\pi\gamma}\frac{(a\sigma(1-m)-b\sigma(m))}{(1-\Delta)}. \tag{4.7}$$

Employing the definitions of the effective resistivities along the x- and y-axes and performing some integrations we find that

$$\rho_x = \rho_2\frac{\sigma(1-m)}{\sigma(m)}\sqrt{\frac{1+\Delta}{1-\Delta}}, \qquad \rho_y = \rho_2\frac{\sigma(m)}{\sigma(1-m)}\sqrt{\frac{1+\Delta}{1-\Delta}}. \tag{4.8}$$

The parameter $\sigma(m)$, defined as

$$\sigma(m) = \frac{(2/\pi)K(m)}{P_{\lambda-(1/2)}(1-2m)}, \tag{4.9}$$

appears throughout; $P_\nu(z)$ is the Legendre function of the first kind. The ratio $\sigma(m)/\sigma(1-m)$ actually appears in all of the expressions associated with effective parameters and is

$$\frac{\sigma(m)}{\sigma(1-m)} = \frac{l}{h}\frac{P_{\lambda-(1/2)}(2m-1)}{P_{\lambda-(1/2)}(1-2m)}; \tag{4.10}$$

the geometric dependence is encapsulated in the l/h terms and, of course, in m, and the material dependence in each phase is encapsulated in λ. An important special case is when $h = l$, that is square checkerboards, then this ratio is simply unity and the expressions for the effective parameters simplify. Another limiting case is high-contrast media, that is, $\rho_2 \gg \rho_1, \rho_3$, then $\lambda \sim 1/2$ and the ratio is then just l/h.

Other explicit results can be found for ρ, the complex representation for the effective resistivity tensor, and for D, the effective energy dissipation. For ρ we could evaluate the integrals explicitly using results derived in Obnosov (1996). Alternatively, one notes that

$$\begin{aligned}\int_\Omega \rho_p w_p(z)\,\mathrm{d}A &= \int_{-l}^{l}\int_{-h}^{h}\rho_p[w_{px} - \mathrm{i}w_{py}]\,\mathrm{d}y\mathrm{d}x \\ &= \int_{-l}^{l} 2ha\rho_x\,\mathrm{d}x - \int_{-h}^{h} 2lb\rho_y\,\mathrm{d}y = 4lh(a\rho_x - \mathrm{i}b\rho_y),\end{aligned}$$

and

$$\int_\Omega w_p(z)\,\mathrm{d}A = \int_{-l}^{l}\int_{-h}^{h}[w_{px} - \mathrm{i}w_{py}]\,\mathrm{d}y\mathrm{d}x = 4lh(a - \mathrm{i}b).$$

Thus,

$$\rho = \frac{a\rho_x - \mathrm{i}b\rho_y}{a - \mathrm{i}b} = \rho_2\sqrt{\frac{1+\Delta}{1-\Delta}}\left[\frac{a(\sigma(1-m)/\sigma(m)) - \mathrm{i}b(\sigma(m)/\sigma(1-m))}{a - \mathrm{i}b}\right]. \quad (4.11)$$

The energy dissipation is calculated using integrals from Obnosov (1996) as

$$D = \rho_2\sqrt{\frac{1+\Delta}{1-\Delta}}\left[a^2\frac{\sigma(1-m)}{\sigma(m)} + b^2\frac{\sigma(m)}{\sigma(1-m)}\right]. \quad (4.12)$$

5. Asymptotic limiting cases

Several limiting cases emerge, either with fewer phases when we can compare with recent results or in cases when there is high contrast between the phases, or geometrically the cells within the checkerboards are square or long and thin. Some aspects of these cases are explored in this section.

(*a*) *Square checkerboards*

For square checkerboards, $h = l$, there are substantial simplifications and, for instance, D is just

$$D = \rho_2\sqrt{\frac{1+\Delta}{1-\Delta}}(a^2 + b^2), \quad (5.1)$$

which reduces to the well-known Keller (1964), Dykhne (1971) result when $\rho_1 = \rho_3$. The crucial parameter here is now just Δ and we can, for instance, set $\rho_3 \to \infty$ and have one cell with an infinite resistivity and $\Delta \sim (1+\epsilon_2)^{-1}$. Results of this nature characterizing the behaviour near junctions between corners with high-contrast media can be useful when used in network approximations (Borcea & Papanicolaou 1998) and can allow one to extend asymptotic results to three dimensions (Keller 1987).

(*b*) *Two-phase checkerboards*

There are two sub-cases here.

Case (i). $\rho_1 = \rho_3$. We then have a chessboard structure; the following simplifications ensue: $\epsilon_3 = 1/\epsilon_2$, $\epsilon_2 = \epsilon$ with $\Delta = (1-\epsilon)/(1+\epsilon)$:

$$\left.\begin{aligned} w_1(\zeta) &= \alpha\mathrm{e}^{\mathrm{i}\pi\gamma}\zeta^{-2\lambda} + \beta\mathrm{e}^{-\mathrm{i}\pi\gamma}\zeta^{+2\lambda}, \\ w_2(\zeta) &= \mathrm{i}\sqrt{\frac{1+\Delta}{1-\Delta}}[\alpha\mathrm{e}^{-\mathrm{i}\pi\gamma}\zeta^{-2\lambda} - \beta\mathrm{e}^{\mathrm{i}\pi\gamma}\zeta^{+2\lambda}], \end{aligned}\right\} \quad (5.2)$$

$$w_3(\zeta) = -\alpha\mathrm{e}^{-3\mathrm{i}\pi\gamma}\zeta^{-2\lambda} - \beta\mathrm{e}^{+3\mathrm{i}\pi\gamma}\zeta^{+2\lambda}, \quad (5.3)$$

$$w_4(\zeta) = -\mathrm{i}\sqrt{\frac{1+\Delta}{1-\Delta}}[\alpha\mathrm{e}^{3\mathrm{i}\pi\gamma}\zeta^{-2\lambda} - \beta\mathrm{e}^{-3\mathrm{i}\pi\gamma}\zeta^{+2\lambda}]. \quad (5.4)$$

For periodic media the real constants are

$$\alpha = \frac{(a\cos\pi\lambda + b)}{2\sin\pi\gamma}, \qquad \beta = \frac{(a\cos\pi\lambda - b)}{2\sin\pi\gamma}, \tag{5.5}$$

thus, the effective resistivities along the x- and y-axes are

$$\rho_x = \frac{2\rho_1\rho_2}{(\rho_1+\rho_2)}, \qquad \rho_y = \tfrac{1}{2}(\rho_1+\rho_2). \tag{5.6}$$

These are the results one would get from a simple electrical resistance analogy; this network approximation and viewpoint is often of considerable use, see recent work by Borcea & Papanicolaou (1998). For checkerboard bi-periodic media the constants are modified to

$$\alpha = \frac{\cos\pi\lambda}{2\sin\pi\gamma}(a\sigma(1-m)+b\sigma(m)), \qquad \beta = \frac{\cos\pi\lambda}{2\sin\pi\gamma}(a\sigma(1-m)-b\sigma(m)). \tag{5.7}$$

The effective resistivities along the x- and y-axes are

$$\rho_x = \sqrt{\rho_1\rho_2}\frac{\sigma(1-m)}{\sigma(m)}, \qquad \rho_y = \sqrt{\rho_1\rho_2}\frac{\sigma(m)}{\sigma(1-m)}, \tag{5.8}$$

which recovers the results in Obnosov (1996). One can similarly evaluate ρ and D and show that these also correspond to this limiting case.

Case (ii). $\rho_1 = \rho_2 = \rho_4$. We have isolated rectangular inclusions embedded within a different phase; the following simplifications ensue: $\epsilon_2 = 1$, $\epsilon_3 = \epsilon$ with $\Delta = (\epsilon-1)/2(1+\epsilon)$. The explicit solutions for w_1 are w_3 are

$$\left.\begin{aligned} w_1(\zeta) &= \alpha \mathrm{e}^{\mathrm{i}\pi\gamma}\zeta^{-2\lambda} + \beta \mathrm{e}^{-\mathrm{i}\pi\gamma}\zeta^{+2\lambda}, \\ w_3(\zeta) &= -(1-2\Delta)[\alpha \mathrm{e}^{-3\mathrm{i}\pi\gamma}\zeta^{-2\lambda} + \beta \mathrm{e}^{3\mathrm{i}\pi\gamma}\zeta^{+2\lambda}], \end{aligned}\right\} \tag{5.9}$$

where, of course, $w_2 = w_4 = w_1$, and w_1 holds in this extended region. Using these we rapidly deduce that for periodic media the real constants are

$$\alpha = \frac{1}{2\cos\pi\gamma}\left(a + \frac{b}{\cos\pi\lambda}\right), \qquad \beta = \frac{1}{2\cos\pi\gamma}\left(a - \frac{b}{\cos\pi\lambda}\right). \tag{5.10}$$

Thus, after integration, the effective resistivities along the x- and y-axes are

$$\rho_x = \frac{\rho_1}{2}\frac{(\rho_1+3\rho_3)}{(\rho_1+\rho_3)}, \qquad \rho_y = \frac{2\rho_1(\rho_1+\rho_3)}{(3\rho_1+\rho_3)}. \tag{5.11}$$

For checkerboard bi-periodic media the real constants change to

$$\alpha = \frac{(a\sigma(1-m)+b\sigma(m))}{2\cos\pi\gamma}, \qquad \beta = \frac{(a\sigma(1-m)-b\sigma(m))}{2\cos\pi\gamma}, \tag{5.12}$$

with the effective resistivities along the x- and y-axes as

$$\rho_x = \rho_1\frac{\sigma(1-m)}{\sigma(m)}\sqrt{\frac{(3\rho_3+\rho_1)}{(\rho_3+3\rho_1)}}, \qquad \rho_y = \rho_1\frac{\sigma(m)}{\sigma(1-m)}\sqrt{\frac{(3\rho_3+\rho_1)}{(\rho_3+3\rho_1)}}. \tag{5.13}$$

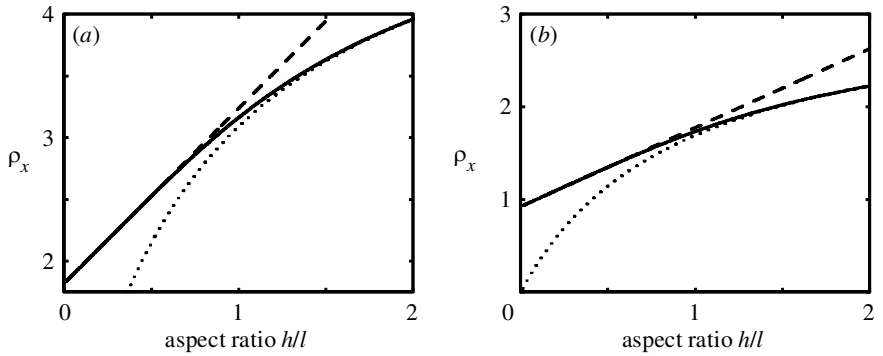

Figure 7. The exact (solid line) and asymptotic (dotted and dashed lines) expressions (5.14) and (5.15) for ρ_x versus h/l. (*a*) $\rho_1 = 10$, $\rho_2 = 0.1$; (*b*) $\rho_1 = 0.5$, $\rho_2 = 6$.

This recovers the results of Obnosov (1999*a*); it is important to note that the results there were deduced in a totally different manner using homogeneous $\mathcal{R}$-linear conjugation Riemann boundary-value problems. It is intriguing that these solutions can be found using the present approach; it is suggestive that many $\mathcal{R}$-linear conjugation Riemann boundary-value problems are actually relatively simple problems that have been mangled and contorted by some conformal mapping such that their final form looks quite formidable.

(*c*) *Thin strips*

The asymptotic limit as $h \ll l$, i.e. long thin strips, is also inviting. Here the parameter m can be found to behave asymptotically as $m \sim 1 - 16\exp(-\pi l/h)$, and this is reasonably accurate even for h/l relatively large, 0.8 say. The other limit when $h \gg l$ can also be approached and then $m \sim 16\exp(-\pi h/l)$. Both these asymptotic expressions for m are shown versus the exact solution in figure 6.

Since we have the exact solutions to hand, we can explicitly investigate this limit using asymptotic representations of the Legendre and elliptic functions. For the special case (i) of § 5 *b*, i.e. when $\rho_1 = \rho_3$, we consider ρ_x. The range of validity of the asymptotic expression for m is suggestive that expansions such as

$$\rho_x \sim \frac{2\rho_1\rho_2}{(\rho_1+\rho_2)}\left[1 - \frac{h}{\pi l}\left(2\gamma + 2\psi(\tfrac{1}{2}+\lambda) + \pi\cot[\pi(\tfrac{1}{2}+\lambda)] + 4\log 2\right)\right] + O(\exp(-\pi l/h)), \quad \text{for } h \ll l, \quad (5.14)$$

will be good over a wide range of h, l and not just for $h \ll l$; indeed this appears to be the case, sample values are shown in figure 7. In (5.14) the parameter γ is now Euler's constant and ψ is the Psi function defined in the usual manner (Abramowitz & Stegun 1969). Similarly, if $h \gg l$ one finds that

$$\rho_x \sim \frac{(\rho_1+\rho_2)}{2}\left[1 - \frac{l}{\pi h}(2\gamma + 2\psi(\tfrac{1}{2}+\lambda) + \pi\cot[\pi(\tfrac{1}{2}+\lambda)] + 4\log 2)\right]^{-1} + O(\exp(-\pi h/l)), \quad \text{for } h \gg l. \quad (5.15)$$

Comparative plots are shown in figure 7.

These asymptotic approximations are excellent versus the full solution. Similar figures can be shown for ρ_y and for the more complicated three-phase media, but these lend nothing new to the discussion. It is also interesting to note that Gautesen's (1988) asymptotic study of the integral equation representations underlying a two-phase checkerboard also led to expressions containing similar combinations of γ and the ψ function; it is now clear from whence these combinations appear.

It also suggests that there is an asymptotic approach to the full problem which would generate these approximations directly, and that this might be useful to pursue for more complicated geometries; this is currently under investigation.

6. Concluding remarks

Previous exact analyses of two-phase media have used solutions to so-called $\mathcal{R}$-linear conjugation Riemann boundary-value problems, also known as Markushevich problems. Here we demonstrate that, at least for checkerboard media, that approach is redundant. The contortions involved in the underlying conformal mapping mean that if one attempts to solve the bi-periodic boundary-value problem directly, then it appears to be extremely complicated; doubly periodic boundary-value problems involving Jacobi elliptic functions are not to be approached by the faint-hearted. It may well be the case that many other Markushevich problems can be explicitly solved once one realizes that there are underlying simplifications to be exploited.

The approach whereby one begins with a simple problem and then one uses subsequent mappings to this to generate periodic and bi-periodic eigensolutions should be of wider value. Indeed, many other model effective media problems of varying complexity, and involving more phases, can be treated in the manner we outline here; for instance, diamond tilings, media involving cracks or ribbon-like inclusions, and media that are composed of many phases. Further examples and extensions are currently under investigation. The asymptotic analysis of § 5 *c* also suggests that there is an approximate approach that could exploit matched asymptotic expansions, and this too is under investigation.

The new scheme described herein reproduces recently found results, avoiding considerable contortions and analysis, and we extend those results to a class of three-phase media, thus showing how the two-phase problems emerge as special cases; to our knowledge, these are the first exact doubly periodic three-phase checkerboard results to have been deduced. Indeed, bar some coated circular inclusion problems (Nicorovici *et al*. 1993) and recent results by Obnosov (1992, 1999*b*) they are, to our knowledge, the first exact three-phase effective parameters to be deduced at all.

It is perhaps also worthwhile pointing out that since one now has the exact solutions for w_p in each phase these can be further used to track the motion of specific particles; this should also be investigated further.

I am grateful for the financial support of an EPSRC Advanced Fellowship and I thank Professor Obnosov for useful interactions.

Appendix A. Useful integrals

These integrals are evaluated in Obnosov (1996) and are useful herein:

$$\frac{1}{h}\int_0^h \left(\tanh\frac{\pi \mathrm{i} y}{2h}\right)^{\pm 2\lambda} \mathrm{d}y = \frac{\mathrm{e}^{\pm \mathrm{i}\pi\lambda}}{\cos\pi\lambda}, \quad \frac{1}{l}\int_0^l \left(\tanh\frac{\pi x}{2h}\right)^{\pm 2\lambda} \mathrm{d}x = 1, \quad \text{as } l \to \infty, \tag{A 1}$$

$$\frac{1}{h}\int_0^h \zeta^{\pm 2\lambda}(\mathrm{i}y)\,\mathrm{d}y = \frac{\mathrm{e}^{\pm \mathrm{i}\pi\lambda}}{\sigma(1-m)\cos\pi\lambda}, \quad \frac{1}{l}\int_0^l \zeta^{\pm 2\lambda}(x)\,\mathrm{d}x = \frac{1}{\sigma(m)\cos\pi\lambda}, \tag{A 2}$$

where ζ is defined in (4.5). We also use several integrals that can be deduced from these, such as

$$\frac{1}{h}\int_{-h}^0 \left(\tanh\frac{\pi \mathrm{i}y}{2h}\right)^{\pm 2\lambda}\mathrm{d}y = \frac{\mathrm{e}^{\mp \mathrm{i}\pi\lambda}}{\cos\pi\lambda}, \tag{A 3}$$

which can be deduced using simple transformations. In addition

$$\frac{1}{lh}\int_{\Omega_1} \zeta^{-2\lambda}(z)\,\mathrm{d}A = \frac{\mathrm{i}}{\Delta}\left(\frac{\mathrm{e}^{-\mathrm{i}\pi\lambda}}{\sigma(1-m)} - \frac{1}{\sigma}\right). \tag{A 4}$$

References

Abramowitz, M. & Stegun, I. A. 1969 *Handbook of mathematical functions*. New York: Dover.

Berdichevski, V. L. 1985 The thermal conductivity of chess structures. *VestnMosk. Univ. Mat. Mech.* **40**, 56–63 (in Russian).

Borcea, L. & Papanicolaou, G. C. 1998 Network approximation for transport properties of high contrast materials. *SIAM J. Appl. Math.* **58**, 501–539.

Bruggeman, D. A. G. 1935 Berechnung verschiedener physikalischer Konstanten von heterogenen Substanzen. *Ann. Phys. Lpz.* **24**, 636–679 (in German).

Clark, K. E. & Milton, G. W. 1995 Optimal bounds correlating electric, magnetic and thermal properties of two-phase, two-dimensional composites. *Proc. R. Soc. Lond.* A **448**, 161–190.

Craster, R. V. 1997 The solution of a class of free boundary problems. *Proc. R. Soc. Lond.* A **453**, 607–630.

Craster, R. V. & Obnosov, Y. V. 2000 Four phase periodic composites. *SIAM J. Appl. Math.* (Submitted.)

Dykhne, A. M. 1971 Conductivity of a two-dimensional two-phase system. *Sov. Phys. JETP* **32**, 63–65.

Gautesen, A. K. 1988 The effective conductivity of a composite-material with a periodic rectangular geometry. *SIAM J. Appl. Math.* **48**, 393–404.

Helsing, J. 1991 Transport properties of two-dimensional tilings with corners. *Phys. Rev.* B **44**, 11 667–11 682.

Keller, J. B. 1963 Conductivity of a medium containing a dense array of perfectly conducting spheres or cylinders or nonconducting cylinders. *J. Appl. Phys.* **34**, 991–993.

Keller, J. B. 1964 A theorem on the conductivity of a composite medium. *J. Math. Phys.* **5**, 548–549.

Keller, J. B. 1987 Effective conductivity of periodic composites composed of two very unequal conductors. *J. Math. Phys.* **28**, 2516–2520.

Lawden, D. F. 1989 *Elliptic functions and applications*. Springer.

Maxwell, J. C. 1904 *A treatise on electricity and magnetism*. Oxford University Press.

Mendelson, K. S. 1975 A theorem on the effective conductivity of a two-dimensional heterogeneous medium. *J. Appl. Phys.* **46**, 4740–4741.

Milton, G. W. & Golden, K. 1990 Representations for conductivity functions of multicomponent composites. *Commun. Pure Appl. Math.* **43**, 647–671.

Milton, G. W., McPhedran, R. C. & McKenzie, D. R. 1981 Transport properties of intersecting cylinders. *Appl. Phys.* **25**, 23–30.

Mityushev, V. V. 1997 Transport properties of double-periodic arrays of circular cylinders. *Z. Angew. Math. Mech.* **77**, 115–120.

Nicorovici, N. A., McPhedran, R. C. & Milton, G. W. 1993 Transport properties of a three-phase composite material: the square array of coated cylinders. *Proc. R. Soc. Lond.* A **442**, 599–620.

Obnosov, Y. V. 1992 Solution of certain boundary problems of $\mathcal{R}$-linear conjugation with piecewise constant coefficients. *Russ. Math. (Izv. VUZ)* **36**, 38–47.

Obnosov, Y. V. 1996 Exact solution of a boundary-value problem for a rectangular checkerboard field. *Proc. R. Soc. Lond.* A **452**, 2423–2442.

Obnosov, Y. V. 1999*a* Periodic heterogeneous structures: new explicit solutions and effective characeristics of refraction of an imposed field. *SIAM J. Appl. Math.* **59**, 1267–1287.

Obnosov, Y. V. 1999*b* Seepage refraction in a semicircular lens located at the boundary of two porous massifs. *J. Appl. Math. Mech.* **62**, 749–762.

Rayleigh, J. W. 1892 On the influence of obstacles arranged in rectangular order upon the properties of the medium. *Phil. Mag.* **34**, 481–502.

Talbot, D. R. S. & Willis, J. R. 1994 Upper and lower bounds for the overall properties of a nonlinear composite dielectric. I. Random microgeometry. *Proc. R. Soc. Lond.* A **447**, 365–384.

Torquato, S. 1991 Random heterogeneous media: microstructure and improved bounds on effective properties. *Appl. Mech. Rev.* **44**, 37–76.